Article

Cell Reports

PI3K/AKT Signaling Regulates H3K4 Methylation in Breast Cancer

Graphical Abstract

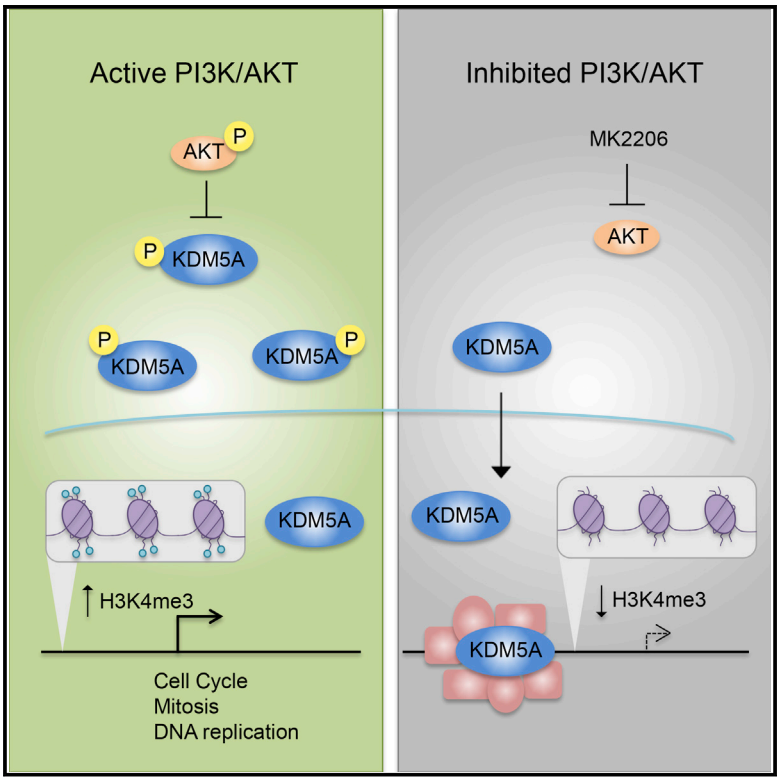

Authors

Jennifer M. Spangle, Koen M. Dreijerink, Anna C. Groner, ..., Jean J. Zhao, Thomas M. Roberts, Myles Brown

Correspondence

thomas_roberts@dfci.harvard.edu (T.M.R.), myles_brown@dfci.harvard.edu (M.B.)

In Brief

Spangle et al. report that PI3K/AKT pathway activation increases H3K4 trimethylation in preclinical models of breast cancer. They show that the H3K4 demethylase KDM5A is an AKT target that cooperates with AKT to increase the expression of cell-cycle genes associated with advanced-stage breast cancer.

Highlights

- PI3K/AKT pathway activation increases H3K4 trimethylation in models of breast cancer
- AKT phosphorylates the H3K4-demethylase KDM5A and directs it to the cytoplasm
- AKT and KDM5A cooperate to regulate the expression of cell-cycle genes
- Expression of AKT/KDM5A-regulated genes is associated with advanced-stage breast cancer

Accession Numbers

GSE80594

Spangle et al., 2016, Cell Reports *15*, 2692–2704
June 21, 2016
http://dx.doi.org/10.1016/j.celrep.2016.05.046

OPEN ACCESS
CellPress

Cell Reports
Article

PI3K/AKT Signaling Regulates H3K4 Methylation in Breast Cancer

Jennifer M. Spangle,[1,2] Koen M. Dreijerink,[3,4] Anna C. Groner,[3,4] Hailing Cheng,[1,5] Carolynn E. Ohlson,[1] Jaime Reyes,[3] Charles Y. Lin,[3] James Bradner,[3] Jean J. Zhao,[1,2] Thomas M. Roberts,[1,2,*] and Myles Brown[3,4,*]
[1]Department of Cancer Biology, Dana Farber Cancer Institute, 44 Binney Street, Boston, MA 02115, USA
[2]Department of Biological Chemistry and Molecular Pharmacology, Harvard Medical School, 44 Binney Street, Boston, MA 02115, USA
[3]Department of Medical Oncology, Dana Farber Cancer Institute, 450 Brookline Avenue, Boston, MA 02115, USA
[4]Department of Medicine, Harvard Medical School, 450 Brookline Avenue, Boston, MA 02115, USA
[5]Present address: Cancer Institute, The Second Hospital of Dalian Medical University, 116044 Dalian, China
*Correspondence: thomas_roberts@dfci.harvard.edu (T.M.R.), myles_brown@dfci.harvard.edu (M.B.)
http://dx.doi.org/10.1016/j.celrep.2016.05.046

SUMMARY

Post-translational histone H3 modifications regulate transcriptional competence. The mechanisms by which the epigenome is regulated in response to oncogenic signaling remain unclear. Here we show that H3K4me3 is increased in breast tumors driven by an activated PIK3CA allele and that inhibition of PI3K/AKT signaling reduces promoter-associated H3K4me3 in human breast cancer cells. We show that the H3K4 demethylase KDM5A is an AKT target and that phosphorylation of KDM5A regulates its nuclear localization and promoter occupancy. Supporting a role for KDM5A in mediating PI3K/AKT transcriptional effects, the decreased expression in response to AKT inhibition of a subset of cell-cycle genes associated with poor clinical outcome is blunted by KDM5A silencing. Our data identify a mechanism by which PI3K/AKT signaling modulates the cancer epigenome through controlling H3K4 methylation and suggest that KDM5A subcellular localization and genome occupancy may be pharmacodynamic markers of the activity of PI3K/AKT inhibitors currently in clinical development.

INTRODUCTION

The PI3K/AKT signaling pathway is frequently activated in human cancers. PI3K phosphorylation of PIP_2 to PIP_3 promotes the phosphorylation and activation of AKT (Engelman et al., 2006; Thorpe et al., 2015). AKT-mediated substrate phosphorylation regulates the transcription and translation of genes required for cellular growth, metabolism, and survival; critical events in transformation and oncogenesis (Manning and Cantley, 2007). Constitutive activation of the PI3K/AKT pathway occurs in more than 50% of human breast cancers, most commonly through mutational activation of the *PIK3CA* gene, mutational activation or amplification of *AKT1*, *AKT2*, or *AKT3*, or functional loss of the lipid phosphatase *PTEN*, whose function counteracts that of PI3K (Cancer Genome Atlas Network, 2012). The frequency of PI3K pathway alterations in human cancers has prompted the development of PI3K-pathway-specific inhibitors, with recent focus on pan-PI3K, isoform-selective PI3K, and AKT inhibitors (Cancer Genome Atlas Network, 2012). Current and recent clinical trials evaluating PI3K-inhibitor monotherapy in solid tumors demonstrate limited efficacy and durability as response rates are relatively low, and tumors frequently recur (Juric et al., 2015; Rodon et al., 2013). A better understanding of the mechanisms by which activated PI3K promotes cancer and informative pharmacodynamic markers of PI3K/AKT inhibitor activity is needed to rationally design effective combination therapeutics involving PI3K inhibitors.

The role of chromatin modification and the induction of a transcriptionally competent state in PI3K-mediated oncogenesis are not well understood. AKT phosphorylates EZH2, an H3K27 histone methyltransferase, inhibiting EZH2 methyltransferase activity and reducing H3K27 trimethylation (H3K27me3) (Cha et al., 2005). AKT-mediated EZH2 phosphorylation also enhances EZH2 function as an oncogenic transcriptional co-activator by associating with androgen receptor and other transcription factors (Xu et al., 2012). Phosphorylation of the polycomb repressive complex 1 (PRC1) component BMI1 by AKT enables PI3K/AKT-mediated epigenetic repression of the *CDKN2A* locus (Liu et al., 2012). AKT activation counteracts induction of p53-dependent senescence through the phosphorylation of the histone acetyltransferase MOZ (Rokudai et al., 2013). It is currently unknown whether PI3K/AKT regulates the function of additional chromatin modifiers and, if so, whether this regulation is important for oncogenic growth.

Changes to the chromatin landscape are associated with cancer development (Kandoth et al., 2013). Clinical data indicate that H3K4me3 may be elevated in breast, kidney, and colon cancers and correlates with a poor clinical outcome (Benard et al., 2014; Liu et al., 2012; Mungamuri et al., 2013). The H3K4 histone demethylase KDM5A/JARID1A/RBP2 functions as a transcriptional repressor by removing di- and tri-methyl groups (Christensen et al., 2007; Klose et al., 2007). Originally characterized as binding to the retinoblastoma protein (RB1), KDM5A regulates RB1-dependent differentiation and senescence (Benevolenskaya et al., 2005; Lopez-Bigas et al., 2008). Overlapping KDM5A and E2F binding sites suggests some RB1-dependent cell-cycle regulation occurs via KDM5A (Lopez-Bigas et al.,

2008). KDM5A association with the Notch/RBP-J repressor complex, Myc, Mad1, and HDACs, suggests KDM5A may have diverse oncogenic functions (Ge et al., 2010; Liefke et al., 2010; Secombe et al., 2007). Loss of KDM5A expression has been shown to reduce cell proliferation, apoptosis, and tumorigenesis in cell culture and in vivo models (Cao et al., 2014b; Hou et al., 2012), but these activities are independent of KDM5A catalytic function. KDM5A was reported to mediate a drug resistant state in breast and lung cancer cells characterized by EGFR mutation when treated with tyrosine kinase inhibitors (Hou et al., 2012; Sharma et al., 2010).

Here, we demonstrate that PI3K/AKT modulates H3K4me3 and identify a mechanism by which PI3K/AKT regulates KDM5A. We show that KDM5A subcellular localization and genome occupancy is dependent on PI3K/AKT in breast cancer cell lines and murine tumor models. Moreover, PI3K/AKT-dependent transcriptional regulation of a set of genes associated with cell-cycle regulation requires KDM5A. Finally, we show that AKT/KDM5A-regulated gene expression is associated with breast cancer progression and is a predictor of poor clinical outcome.

RESULTS

PI3K/AKT Activation Mediates H3K4 Methylation

Previous studies demonstrated that AKT-mediated EZH2 phosphorylation reduces H3K27me3 and enhances transcription (Cha et al., 2005). High H3K4me3 and low H3K27 methylation are indicative of a poor clinical outcome in some cancers (Benard et al., 2014; Cao et al., 2014a; Liu et al., 2012; Mungamuri et al., 2013; Wei et al., 2008). We first examined if AKT regulates H3K4 methylation in breast tumors. Primary murine mammary tumors driven by doxycycline (dox)-inducible expression of the human $PIK3CA^{H1047R}$ (Liu et al., 2011) show an increase in H3K4me3 abundance upon PI3K activation (Figure 1A). Loss of $PIK3CA^{H1047R}$ expression upon dox withdrawal or treatment with the pan-PI3K inhibitor GDC-0941 (GDC) is sufficient to reduce H3K4me3 in these tumors (Figures 1A and 1B). We next analyzed H3K4me1/2/3 in a human breast cancer cell line expressing the $PIK3CA^{H1047R}$ gene, T47D, following treatment with the AKT inhibitor MK2206 (MK) (Figure 1C), the pan-PI3K inhibitors GDC or BKM120 (BKM), or the p110α and p110β isoform-specific inhibitors BYL719 (BYL) and AZD6482 (AZD), respectively (Figures 1D and 1E). PI3K or AKT inhibition was sufficient to reduce H3K4me3 over a time course, with maximum reduction of H3K4me3 detectable after 72 hr of AKT/PI3K inhibition (Figures 1C–1E). Similar results were obtained in other breast cancer lines, suggesting that the effect is independent of the mechanism by which the PI3K pathway has been activated including *HER2* amplification/overexpression (BT474, MDA-MB-361, Cal-148), *PIK3CA* mutation (T47D, MCF7, BT474, MDA-MB-361), or *PTEN* loss (ZR751, BT549, MDA-MB-468, HCC1937, HCC38, Cal-148) (Figures 1F and 1G). In addition, the status of *RB1* or *TP53* did not impact the ability of AKT inhibition to reduce H3K4me3. Moreover, H3K4me3 is reduced by AKT inhibition in breast cell lines in which the AKT substrate S6 remains phosphorylated (Figure 1F, HCC1937; HCC38; BT549), suggesting the signal mediating the reduction in H3K4me3 originates upstream of S6. Because both the PI3K/AKT and MEK/ERK pathways activate mTORC1, we inhibited mTORC1 and MEK and found that neither was sufficient to reduce H3K4me3 (Figures S1A and S1B), suggesting that AKT alone regulates H3K4 methylation. Additional experiments demonstrate that the ability of PI3K/AKT pathway inhibitors to reduce the levels of H3K4 methylation is independent of their effects on apoptosis or senescence (Figures S1C–S1E). Despite the known interactions between enzymes that regulate H3K4 methylation and RB1, stable *RB1* knockdown does not alter H3K4 methylation (Figure S1F).

AKT Inhibition Decreases Promoter-Associated H3K4me3 and Cell-Cycle Gene Expression

H3K4me3 is abundant near transcriptional start sites (TSSs) and is a mark of active transcription (Santos-Rosa et al., 2002). To determine if AKT regulates promoter-localized H3K4me3, we inhibited AKT and performed H3K4me3 chromatin immunoprecipitation (ChIP), followed by next-generation sequencing (ChIP-seq) over a time course. AKT inhibition reduces H3K4me3 in comparison to vehicle-treated cells as early as 24 hr across all TSSs (Figure 2A). Because PI3K/AKT inhibition also reduces H3K4me2 (Figures 1C–1F), we performed H3K4me2 ChIP-seq but did not detect any significantly regulated genomic loci (data not shown). TSSs were ranked by the change in H3K4me3 following either vehicle or 24 hr AKT inhibition (Figure 2B). AKT inhibition for 24 hr significantly reduces the H3K4me3 near the TSS of 69 genes ($\geq$0.5 log fold decrease), and this loss is maintained through 72 hr AKT inhibition (Figures 2C and S2A). We also inhibited AKT for 24 hr and used RNA sequencing (RNA-seq) to define AKT-regulated transcripts. Gene expression was not globally affected by 24 hr AKT inhibition ($p = 0.20$) (Figure 2D). Gene set enrichment analysis (GSEA) of the RNA-seq dataset demonstrates AKT inhibition reduces transcription of cell-cycle, mitotic, and DNA replication-associated genes (Figure 2E). AKT or PI3K inhibition is sufficient to reduce the abundance of H3K4me3 at promoters of AKT-regulated genes, which is detectable as early as 2 hr following AKT inhibition and up to 24 hr (Figures 2F, 2G, and S2B). In comparison, H3K4me3 of the α-tubulin promoter remains unchanged. An AKT-mediated reduction in regulated gene transcription is detected as early as 12 hr following AKT or PI3K inhibition (Figures 2H, 2I, and S2C). AKT inhibition also reduces the expression of these genes at the protein level (Figure 2J). Promoter-H3K4me3 and transcription of AKT-regulated genes is also reduced with AKT inhibition in MCF7 (Figures S2D and S2E) and ZR-75-1 (Figures S2F and S2G) breast cancer cell lines.

Because PI3K/AKT inhibitors produce cytostatic effects (Juntilla et al., 2009), we tested whether the reduction of the transcription and protein expression of cell-cycle genes after AKT inhibition is a result of epigenomic changes rather than cell-cycle arrest. We found that while PI3K/AKT inhibition decreases H3K4me3, it moderately increases the number of cells in G1 (Figure S3A). We further arrested populations of T47D cells in G1, S, or G2/M. While thymidine/nocodazole treatment with 15.5 hr release enriches cells in G1 with a similar efficiency as AKT inhibition (Figure S3B), it is not sufficient to reduce H3K4me3 (Figure S3C). H3K4me3 was similarly unchanged following

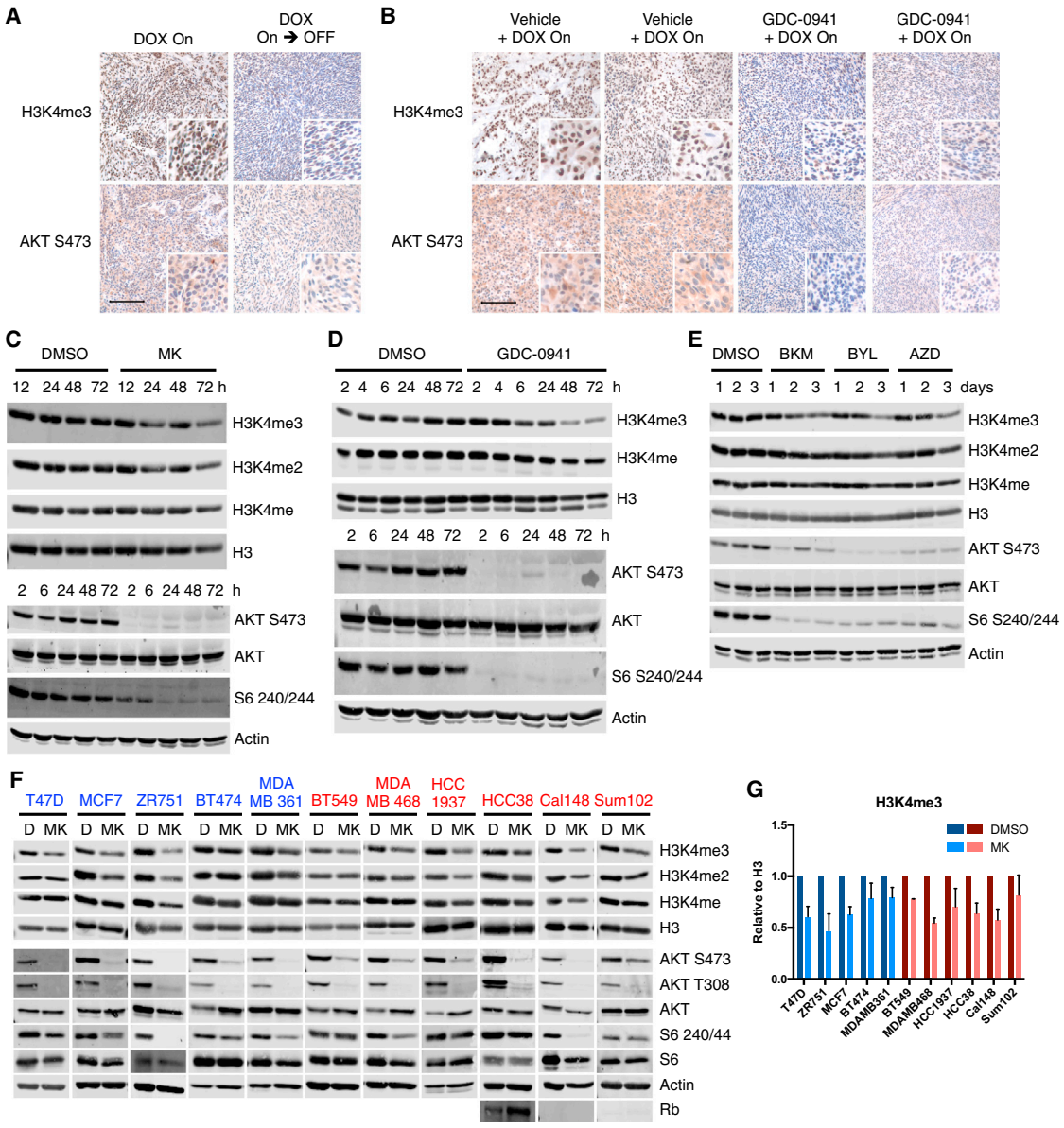

Figure 1. PI3K/AKT Activity Regulates H3K4 Methylation in Breast Cancer

(A) Matched tumor biopsies derived from dox-treated iPIK3CA^{H1047R} mice. A fraction of each tumor was isolated, followed by dox removal and a second biopsy. Sections stained with the indicated antibodies. Randomly selected images shown. Scale bar, 100 μM. n = 3 mice/condition.

(B) Tumors derived from dox-treated iPIK3CA^{H1047R} mice administered vehicle or GDC-0941 for 7 days prior to tumor isolation. Sections stained with the indicated antibodies. Randomly selected images shown. Scale bar, 100 μM. n = 3 mice/condition.

(C) T47D breast cancer cells treated with MK2206 (1 μM) or DMSO for the indicated times and lysates acid extracted. Lysates were immunoblotted with the indicated antibodies.

(D) T47D treated with GDC-0941 (1 μM) or DMSO for the indicated times and lysates acid extracted. Lysates were immunoblotted with the indicated antibodies.

(E) T47D treated with BKM120 (1 μM), BYL-719 (1 μM), AZD (1 μM) or DMSO for the indicated times and lysates acid extracted. Lysates were immunoblotted with the indicated antibodies.

(F) A panel of breast cancer cell lines (blue, luminal; red, basal) was treated with MK2206 (1 μM) or DMSO for 72 hr and lysates acid extracted. Lysates were immunoblotted for the indicated antibodies.

(G) Blot quantification of H3K4me3 abundance from (D). Results are representative of at least three independent experiments. Data are shown as mean ± SEM. See also Figure S1.

arrest in S or G2/M. These results are consistent with the hypothesis that AKT signaling is driving changes to TSS-localized H3K4me3 independently of cell-cycle arrest. We conclude that PI3K/AKT signaling is required for promoter H3K4me3, transcriptional activation, and expression of cell-cycle-promoting genes.

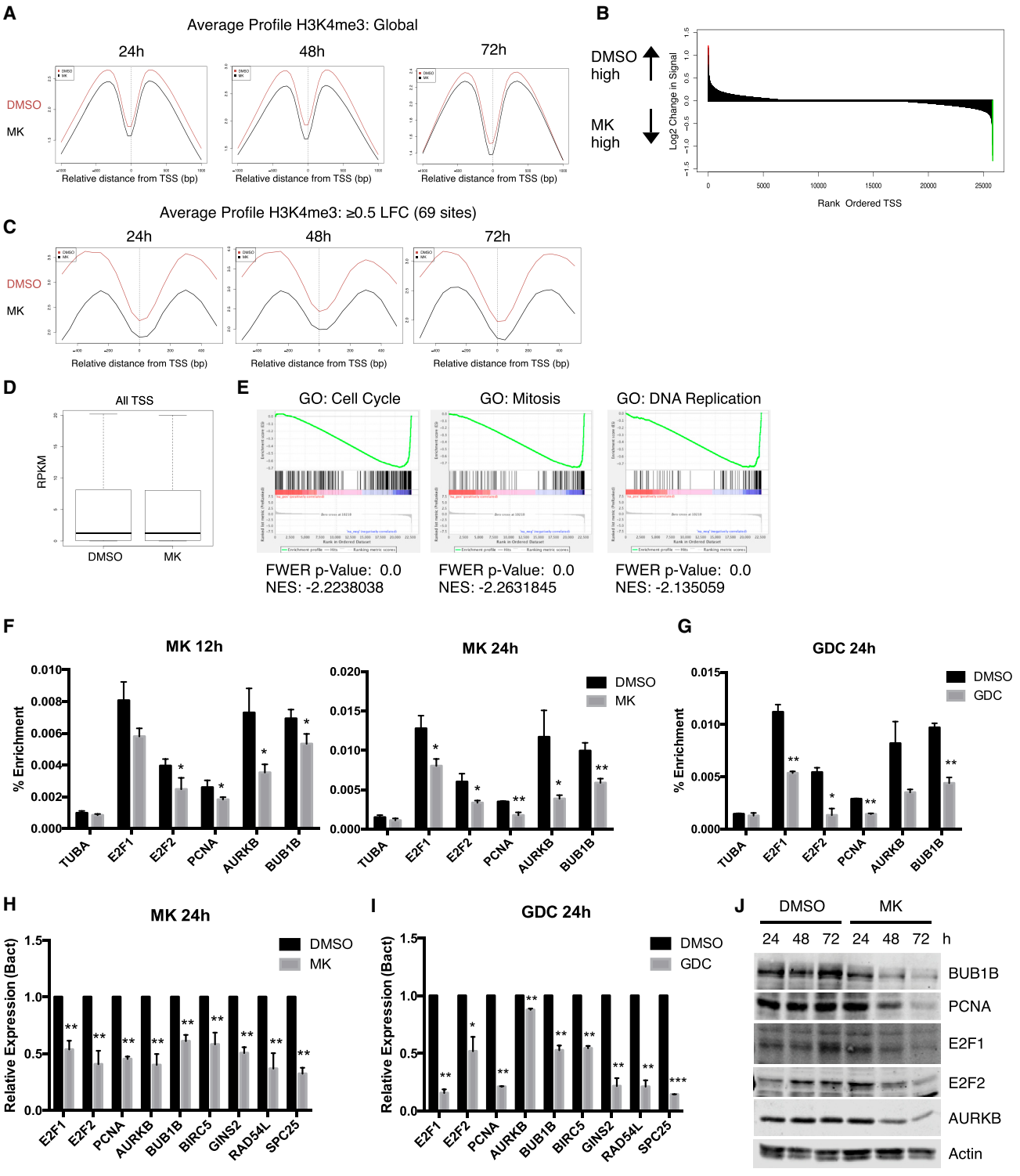

Figure 2. AKT Regulates Promoter-Associated H3K4 Trimethylation and G1 and G2/M Gene Expression

(A) Wave plots of T47D cells treated with MK2206 (1 μM) for the indicated times, harvested and H3K4me3 ChIP-seq. DMSO, red; MK, black. 27,000 TSSs are represented.

(B) Waterfall plot of rank ordered TSSs from (A).

(C) Wave plots of T47D cells treated with MK2206 (μM) for the indicated times, harvested, and H3K4me3 ChIP-seq. DMSO, red; MK, black. TSSs with ≥0.5 log fold change (LFC) H3K4me3 are represented.

(legend continued on next page)

KDM5A Is an AKT Substrate

KDM5 enzymes demethylate di- and tri-methylated H3K4 (Klose et al., 2007). We utilized Scansite to examine whether KDM5 proteins are AKT substrates based on the AKT consensus motif RxRxxS/T (Obenauer et al., 2003; Songyang et al., 1994). Scansite analysis identified five AKT consensus motifs within KDM5A (Figure 3A), all of which are highly conserved among mammals and partially conserved in the divergent *Xenopus* genus (Figure 3B). To investigate whether KDM5A is an AKT target, we generated a compound KDM5A mutant that could not be phosphorylated by AKT at any of the predicted sites ($KDM5A^{S225A,\ T285A,\ S287A,\ T1225A,\ S1255A}$; $KDM5A^{mut5A}$). We immunoprecipitated ectopically expressed wild-type KDM5A or $KDM5A^{mut5A}$ and performed an in vitro kinase assay using recombinant AKT1 in the presence or absence of AKT inhibition. Wild-type KDM5A is phosphorylated by AKT1 and this modification is sensitive to AKT inhibition, whereas $KDM5A^{mut5A}$ is not phosphorylated in the presence of AKT1 (Figure 3C). Wild-type KDM5A is also phosphorylated in cell culture and its phosphorylation is sensitive to AKT inhibition (Figure 3D). In order to investigate the impact of AKT signaling on KDM5A chromatin association, we inhibited AKT and performed KDM5A ChIP-seq. In the absence of AKT inhibition, 95% of KDM5A is TSS localized (±5 kb) (Figure 3E). AKT inhibition for 24 hr increased KDM5A recruitment to TSSs (Figure 3F), coincident with a reduction in TSS H3K4me3 (Figures 2A and S4). These results suggest that AKT-mediated KDM5A phosphorylation enhances KDM5A promoter recruitment.

AKT Regulates KDM5A Subcellular Localization

FOXO phosphorylation by AKT leads to its cytoplasmic retention (Brunet et al., 1999). To investigate whether KDM5A phosphorylation by AKT changes KDM5A subcellular localization, we ectopically expressed wild-type KDM5A and performed KDM5A immunofluorescence in the presence and absence of AKT inhibition. Under normal growth conditions, wild-type KDM5A is both nuclear and cytoplasmic, and pharmacologic AKT inhibition drives KDM5A into the nucleus (Figure 4A). AKT inactivation via serum starvation increases nuclear KDM5A, and growth factor stimulation relocalizes a substantial fraction of wild-type KDM5A to the cytoplasm (Figure 4B). These effects are similar to AKT-mediated FOXO phosphorylation. In contrast, the subcellular localization of $KDM5A^{mut5A}$ that cannot be phosphorylated by AKT is not affected by the modulation of AKT activity through serum starvation/stimulation or pharmacological inhibition (Figure S5A). Biochemical fractionation in T47D cells that stably express wild-type HA-FLAG-KDM5A demonstrates that nuclear localized and chromatin-bound KDM5A increases with AKT inhibition (Figures 4C, S5B, and S5C). In contrast, HA-FLAG-$KDM5A^{mut5A}$ cytoplasmic abundance is reduced, instead shifting into the nuclear compartment in the absence of AKT inhibition (Figures 4D and S5C). Tumors derived from the dox-inducible $PIK3CA^{H1047R}$ murine tumor model further demonstrate that PI3K pathway activation modulates KDM5A subcellular localization. KDM5A strongly localizes to the cytoplasm in PI3K-pathway activated tumors (Figure 4E). Dox removal and thus loss of $PIK3CA^{H1047R}$ transgene expression or treatment with the pan-PI3K inhibitor GDC-0941 is sufficient to reduce cytoplasmic KDM5A localization and promote nuclear KDM5A localization (Figures 4E and 4F).

To determine whether $KDM5A^{mut5A}$ insensitivity to AKT-mediated phosphorylation and subsequent subcellular redistribution increases $KDM5A^{mut5A}$ recruitment to the promoters of AKT-regulated genes, we performed HA-ChIP with T47D cells that stably express wild-type HA-FLAG-KDM5A or HA-FLAG-$KDM5A^{mut5A}$. $KDM5A^{mut5A}$ promoter occupancy at AKT-regulated genes is increased in comparison to wild-type KDM5A (Figure 4G). Together, these results suggest KDM5A subcellular localization is partially dependent on its phosphorylation by AKT, and KDM5A phosphorylation by AKT decreases KDM5A recruitment to the promoters of AKT-regulated genes.

AKT/KDM5A-Regulated Gene Expression Is Elevated in Cancers and Is a Predictor of Poor Outcome

To examine the functional significance of KDM5A downstream of PI3K/AKT signaling, we integrated the H3K4me3- and KDM5A-ChIP-seq with the RNA-seq data following AKT inhibition to identify genes regulated by AKT/KDM5A (Figure 5A). KDM5A recruitment after 24 hr AKT inhibition is increased at all TSSs (69 total) characterized by a $\geq$0.5 log fold reduction in H3K4me3 (Figures 2C and 5B). Promoter-localized H3K4me3, transcription, and protein detection of AKT/KDM5A-regulated genes are reduced following PI3K/AKT inhibition (Figures 2F–2J). To investigate whether KDM5A is necessary for the transcription of AKT-regulated genes, we utilized lentiviral shRNA expression vectors to knock down KDM5A in the presence or absence of AKT inhibition and evaluated nascent RNA transcription. Nascent RNA transcription of two direct AKT/KDM5A targets, *AURKB* and *E2F2*, was no longer sensitive to AKT inhibition following KDM5A knockdown (Figure 5C and S5C). Taken together, these data suggest AKT regulates the expression of a set of cell-cycle genes through KDM5A.

(D) Transcript abundance (RNA-seq) in T47D cells treated with DMSO or MK2206 (1 μM) for 24 hr. p = 0.20.
(E) GSEA (GO biological processes) from T47D cells treated with MK2206 (1 μM) for 24 hr and RNA-seq.
(F) T47D cells treated with MK2206 (1 μM) for the indicated times. Cells were harvested; H3K4me3 ChIP performed prior to qPCR at promoter-localized regions for the genes indicated. Data are shown as mean ± SEM; *p ≤ 0.05, **p ≤ 0.01, ***p ≤ 0.001, Student's t test.
(G) T47D cells treated with GDC-0941 (1 μM), 24 hr. Cells were harvested; H3K4me3 ChIP performed prior to qPCR at promoter-localized regions for the genes indicated. Data are shown as mean ± SEM; *p ≤ 0.05, **p ≤ 0.01, ***p ≤ 0.001, Student's t test.
(H) T47D cells treated with MK2206 (1 μM), 24 hr. RNA was isolated prior to qPCR within the gene bodies for the genes indicated. Data are shown as mean ± SEM; *p ≤ 0.05, **p ≤ 0.01, ***p ≤ 0.001, Student's t test.
(I) T47D cells treated with GDC-0941 (1 μM), 24 hr. RNA was isolated prior to qPCR within the gene bodies for the genes indicated. Data are shown as mean ± SEM; *p ≤ 0.05, **p ≤ 0.01, ***p ≤ 0.001, Student's t test.
(J) T47D cells treated with MK2206 (1 μM) for the indicated times. Cell lysates were immunoblotted with the indicated antibodies.
See also Figures S2–S4.

A

Phosphorylation Site	Scansite Score	Scansite %	Z-Score
(+) Ezh2 S21	0.649	2.35%	-2.92
(+) MOZ T369	0.349	0.02%	-5.60
KDM5A T285	0.388	0.07%	-5.25
KDM5A T1225	0.411	0.07%	-5.03
KDM5A T1255	0.551	0.69%	-3.80
KDM5A S225	0.678	3.21%	-2.66
KDM5A S287	0.554	0.72%	-3.76

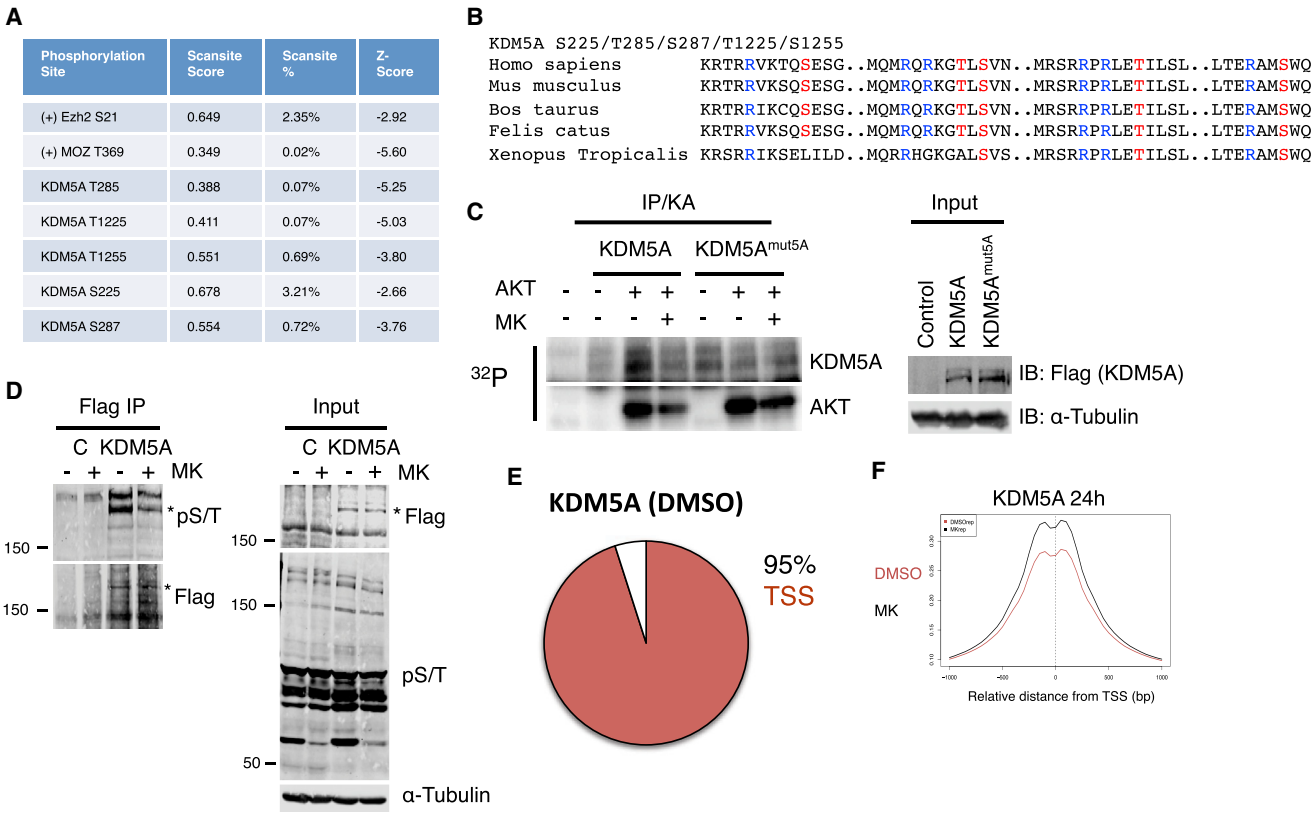

Figure 3. KDM5A Is an AKT Target

(A) Table indicating Scansite prediction of AKT consensus motifs within KDM5A in comparison to positive controls EZH2 and MOZ.

(B) Clustal W sequence alignment of orthologous KDM5A AKT consensus motifs.

(C) An IP/kinase assay was performed after transection of 293T cells with wild-type HA-FLAG-KDM5A or HA-FLAG-KDM5A^{mut5A}. Flag-IP was used to isolate KDM5A, followed by incubation with γ-ATP, recombinant AKT1, and MK2206 (2 μM) where indicated. Transfer of radiolabeled phosphate to KDM5A was detected by phosphorescence. Input cell lysates were immunoblotted with the indicated antibodies.

(D) A FLAG IP was performed after 293T transfection with wild-type HA-FLAG-KDM5A, followed by treatment with MK2206 (1 μM) for 1 hr. FLAG-IP was used to isolate KDM5A followed by immunoblotting with the indicated antibodies. *KDM5A phosphorylated at S/T residues.

(E) Pie chart representing KDM5A genome localization from ChIP-seq data in T47D cells treated with DMSO for 24 hr.

(F) Wave plot of T47D cells treated with MK2206 (1 μM) for 24 hr, harvested, and KDM5A ChIP-seq. DMSO, red; MK, black.

See also Figure S4.

To explore the functional relevance of AKT/KDM5A gene regulation in cancer, the gene expression database Oncomine was queried with the AKT/KDM5A regulated gene set (Rhodes et al., 2004). Expression of these genes is significantly higher in invasive breast carcinoma as compared to normal tissue (Figure 5D) and correlates with metrics of advanced stage disease including increased metastatic event, increased breast cancer recurrence, and increased death within 5 years of initial diagnosis (Figures 5E–5G). Thus, AKT-mediated modulation of promoter H3K4 methylation may be an important component in PI3K-activated oncogenesis.

DISCUSSION

The high frequency of PI3K/AKT pathway alterations in breast and other cancers has led to the clinical development of PI3K pathway inhibitors (Cancer Genome Atlas Network, 2012; Thorpe et al., 2015). To date, the limited efficacy and durability of PI3K inhibitor monotherapy has encouraged the development and testing of combination therapies targeting PI3K. Thus, defining additional mechanisms by which PI3K/AKT contributes to oncogenesis is essential to understanding the mechanics of existing therapies and may support the development of potent and durable PI3K/AKT combination therapies. Here, we demonstrate that PI3K/AKT pathway activation promotes H3K4me3. Further, we demonstrate that the H3K4 demethylase KDM5A is an AKT target and that AKT may collaborate with KDM5A to regulate the expression of a set of cell-cycle genes. This connection between PI3K/AKT signal transduction and the cancer epigenome suggests an additional mechanism by which PI3K/AKT activation may contribute to oncogenesis. We demonstrate that one action of PI3K/AKT inhibitors is to reduce the expression of a subset of cell-cycle-promoting genes, including E2F transcription factors and *AURKB*, and this requires KDM5A. This mechanism is suggestive of nodes within the PI3K/AKT signaling network that could be therapeutically exploited in PI3K-activated

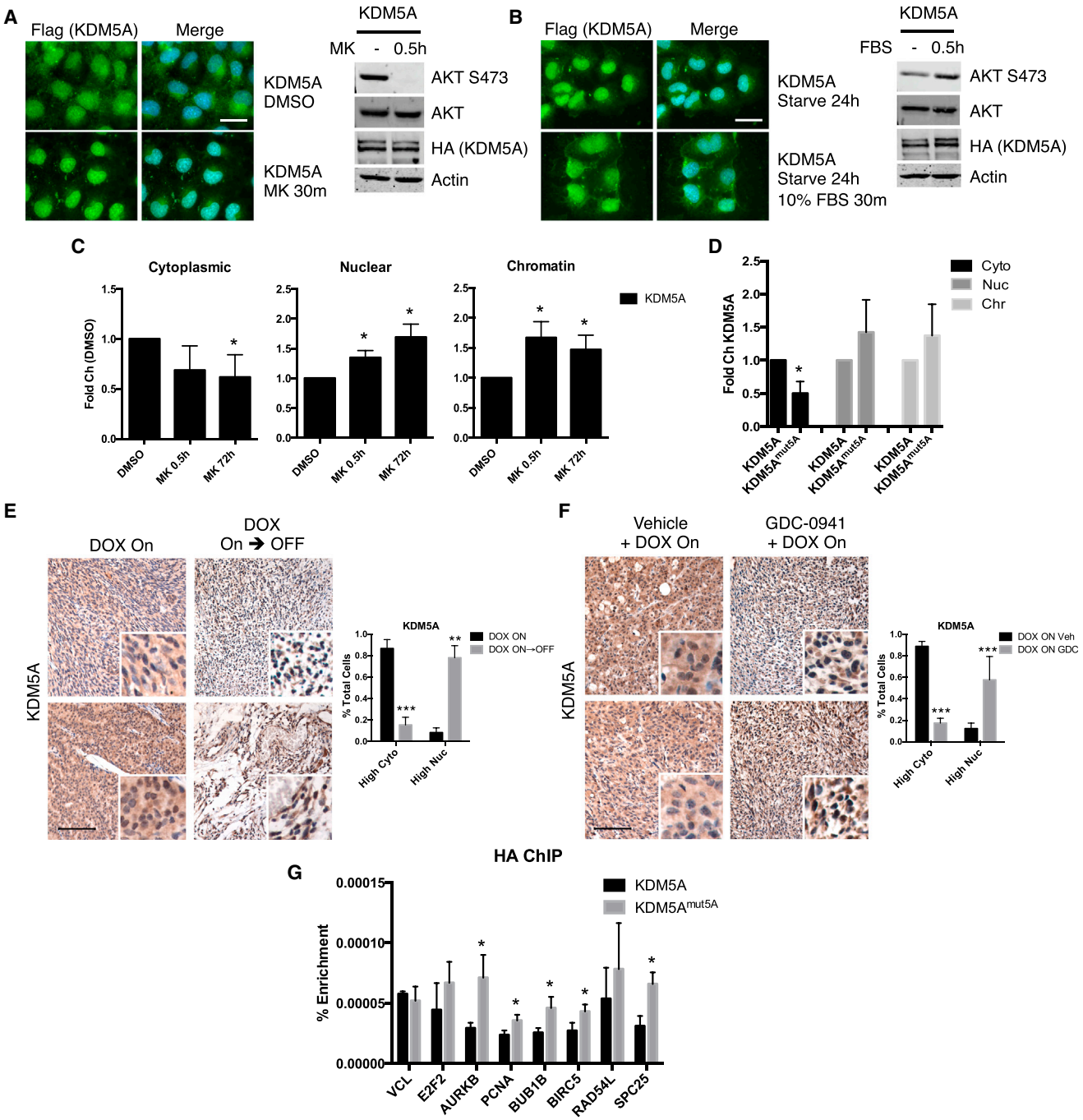

Figure 4. AKT Mediates KDM5A Subcellular Localization

(A) Immunofluorescence and immunoblot analysis were performed after transfection of Cos7 cells with wild-type HA-FLAG-KDM5A. Cells were treated with MK2206 (1 μM) for 0.5 hr. Fixed cells were probed for FLAG (KDM5A), and lysates were probed with the indicated antibody, including HA (KDM5A). Scale bar, 35 μM.

(B) Immunofluorescence and immunoblot analysis were performed after transfection of Cos7 cells with wild-type HA-FLAG-KDM5A. Cells were starved for 24 hr in 0% FBS DMEM and then growth factor stimulated with 10% FBS DMEM for 0.5 hr. Fixed cells were probed for FLAG (KDM5A), and lysates were probed with the indicated antibody, including HA (KDM5A). Scale bar, 35 μM.

(C) T47D cells stably expressing wild-type HA-FLAG-KDM5A were treated with MK2206 (1 μM) for the indicated time and cells were biochemically fractionated. KDM5A subcellular localization was quantified relative to control treatment. n = 3 independent experiments. Data are shown as mean ± SEM. *Student's t test, $p \leq 0.05$.

(legend continued on next page)

breast tumors. Moreover, this mechanism suggests that H3K4me3 and KDM5A subcellular localization could serve as clinical pharmacodynamic markers for PI3K inhibition.

We present a model in which KDM5A phosphorylation by AKT shifts KDM5A subcellular localization from the nuclear and chromatin-bound fractions to the cytoplasm, where it is unable to demethylate H3K4me2/3 (Figure 6). In contrast, non-phosphorylated KDM5A is predominantly nuclear and chromatin-bound. While AKT PH domains predominantly localize AKT to the cellular membrane, phosphorylated AKT is present in the nucleus, where the majority of KDM5A is accessible (Meier et al., 1997). Modulation of KDM5A subcellular localization following PI3K/AKT activation or inhibition supports this model. Together, AKT/KDM5A increase the expression of genes that facilitate cell-cycle progression, which may contribute in part to the increased cellular proliferation frequently observed in PI3K-activated breast cancers. Increased nuclear/chromatin-associated KDM5A, either through AKT inhibition or expression of non-phosphorylatable KDM5A^{mut5A}, enhances KDM5A promoter recruitment and reduces AKT/KDM5A-regulated gene expression. However, biochemical fractionation, immunofluorescence (IF), and immunohistochemistry (IHC) from PI3K-activated mammary tumors and cell lines demonstrate that some, but not all, KDM5A relocalization is dependent on the modulation of PI3K/AKT activity. While these data suggest that the relocalization of a fraction of total KDM5A by AKT might be sufficient to alter gene expression, it is possible that AKT-mediated KDM5A phosphorylation regulates other aspects of chromatin biology—e.g., the association of KDM5A with other chromatin-bound complexes (HDACs, KDM2B, RB1, IKKα/β).

We speculate that nuclear KDM5A may function as a tumor suppressor by demethylating H3K4me3 and thus reducing the transcriptional competence of a subset of cell-cycle-promoting genes. Contrary to our findings, a previous study suggests that breast cancer progression and lung metastasis requires KDM5A expression, but utilization of the H483A demethylase inactive mutant suggests that oncogenic KDM5A activity is independent of its histone demethylase activity (Cao et al., 2014b). Our model suggests AKT-driven KDM5A modulation and potential tumor suppressive function is dependent on KDM5A recruitment to chromatin, and we speculate that KDM5A demethylase activity may be important for this process. We propose that AKT dictates KDM5A function at least in part by regulating its subcellular compartmentalization, and the observed reduction in TSS-associated H3K4me3 following AKT inhibition may be dependent on intact KDM5A demethylase activity. It is likely that KDM5A possesses separable nuclear and cytoplasmic functions, as well as demethylase-dependent and demethylase-independent functions. It is not uncommon that a transcriptional regulator can serve both oncogenic and tumor suppressive functions—e.g., Notch signaling functions as either depending on tissue type (Kopan and Ilagan, 2009). Unconventional functions of histone modifiers, either independent of catalytic activity or dependent of catalytic activity but directed to alternative, non-histone substrates, have recently been uncovered, including non-histone EZH2 and HDAC substrates (Hamamoto et al., 2015; Luo et al., 2000; Xu et al., 2012).

KDM5A and AKT have previously been implicated in cell-cycle regulation via alternative mechanisms. KDM5A promoter occupancy of the cyclin-dependent kinase inhibitors (CDKI) p21^{CIP1}, p27^{kip1}, and p16^{ink4a} suppresses CDKI expression, preventing senescence in gastric and cervical cancer cell lines (Jiping et al., 2013; Zeng et al., 2010). Our results are consistent with these reports by suggesting that AKT promotes proliferative competence via KDM5A phosphorylation and cytoplasmic relocalization. In this model, we propose that AKT-meditated KDM5A phosphorylation and the resulting increased transcription of cell-cycle-promoting genes is an activating event, whereas AKT inhibition is an inhibitory event that may enable KDM5A chromatin recruitment, H3K4 demethylation, and repression of cell-cycle-promoting gene expression. The PI3K/AKT pathway is also an established regulator of the cell cycle by modulating cyclin D translation through mTORC1 (Gera et al., 2004). Moreover, CDK2/cyclin A-mediated AKT S477/T479 phosphorylation and activation fluctuates over the cell cycle, with maximal activity in G2 (Liu et al., 2014). Here, enrichment of breast cancer cells in G2 (or G1 or M phase) did not change H3K4me3, suggesting that AKT phosphorylation at S473 and T308 may be sufficient to modulate KDM5A throughout the cell cycle independently of CDK2/cyclin A. Thus, while it is established that AKT regulates the cell cycle at multiple levels, our results show that this regulation may be mediated in part through effects on the epigenome via KDM5A.

The data presented here demonstrate that PI3K/AKT regulate H3K4 methylation and that PI3K/AKT regulates the transcription of cell-cycle-promoting genes via a KDM5A-dependent mechanism. While KDM5A promoter occupancy is increased at promoters that are also characterized by a reduction in H3K4me3 following AKT inhibition, KDM5A knockdown restores the nascent transcription of only several AKT-regulated genes in response to AKT inhibition (Figure 5C). Moreover, inducible

(D) T47D cells stably expressing wild-type HA-FLAG-KDM5A and HA-FLAG-KDM5A^{mut5A} grown under normal conditions were biochemically fractionated. KDM5A^{mut5A} subcellular localization was quantified relative to wild-type KDM5A. n = 3 independent experiments. Data are shown as mean ± SEM. *Student's t test, $p \leq 0.05$.

(E) Matched tumor biopsies derived from dox-treated iPIK3CA^{H1047R} mice. A fraction of each tumor was isolated and followed by dox removal and a second biopsy. Sections stained with the indicated antibodies. Quantification of cytoplasmic and nuclear staining indicated on the right. Randomly selected images shown. Scale bar, 100 μM. n = 3 mice/condition. Data are shown as mean ± SEM. **$p \leq 0.01$, ***$p \leq 0.0001$, Student's t test.

(F) Tumors derived from dox-treated iPIK3CA^{H1047R} mice administered vehicle or GDC-0941 for 7 days prior to tumor isolation. Sections stained with the indicated antibodies. Quantification of cytoplasmic and nuclear staining indicated on the right. Randomly selected images shown. Scale bar, 100 μM. n = 3 mice/condition. Data are shown as mean ± SEM. ***$p \leq 0.0001$, Student's t test.

(G) Stable T47D cells expressing wild-type HA-FLAG-KDM5A or HA-FLAG-KDM5A^{mut5A} were harvested and HA-ChIP performed prior to qPCR at promoter-localized regions for the genes indicated. Data are shown as mean ± SEM. *Student's t test, $p \leq 0.05$.

See also Figure S5.

A

Rank	Refseq ID	Gene	LFC H3K4me3	LFC mRNA	Limma p-value
1	NM_004217	AURKB	-0.7884595	-1.8677180	1.53E-05
2	NM_001034	RRM2	-0.6901464	-2.2874902	2.22E-04
3	NM_004091	E2F2	-0.9809361	-1.5973477	2.96E-04
4	NM_005225	E2F1	-0.673974	-1.5831691	8.86E-05
5	NM_001211	BUB1B	-0.7048391	-1.4709826	4.47E-04
6	NM_016095	GINS2	-0.5900473	-1.6015749	2.83E-04
7	NM_004526	MCM2	-0.6141432	-1.4200915	1.92E-04
8	NM_182649	PCNA	-0.5315250	-1.5818546	2.70E-04
9	NM_001142548	RAD54L	-0.5746235	-1.2154571	8.19E-03
10	NM_020675	SPC25	-0.5324244	-1.3017978	5.96E-04
11	NM_001029989	KIAA0101	-0.5453364	-0.6953022	6.52E-04
12	NM_001168	BIRC5	-0.5108818	-1.2982494	5.81E-04

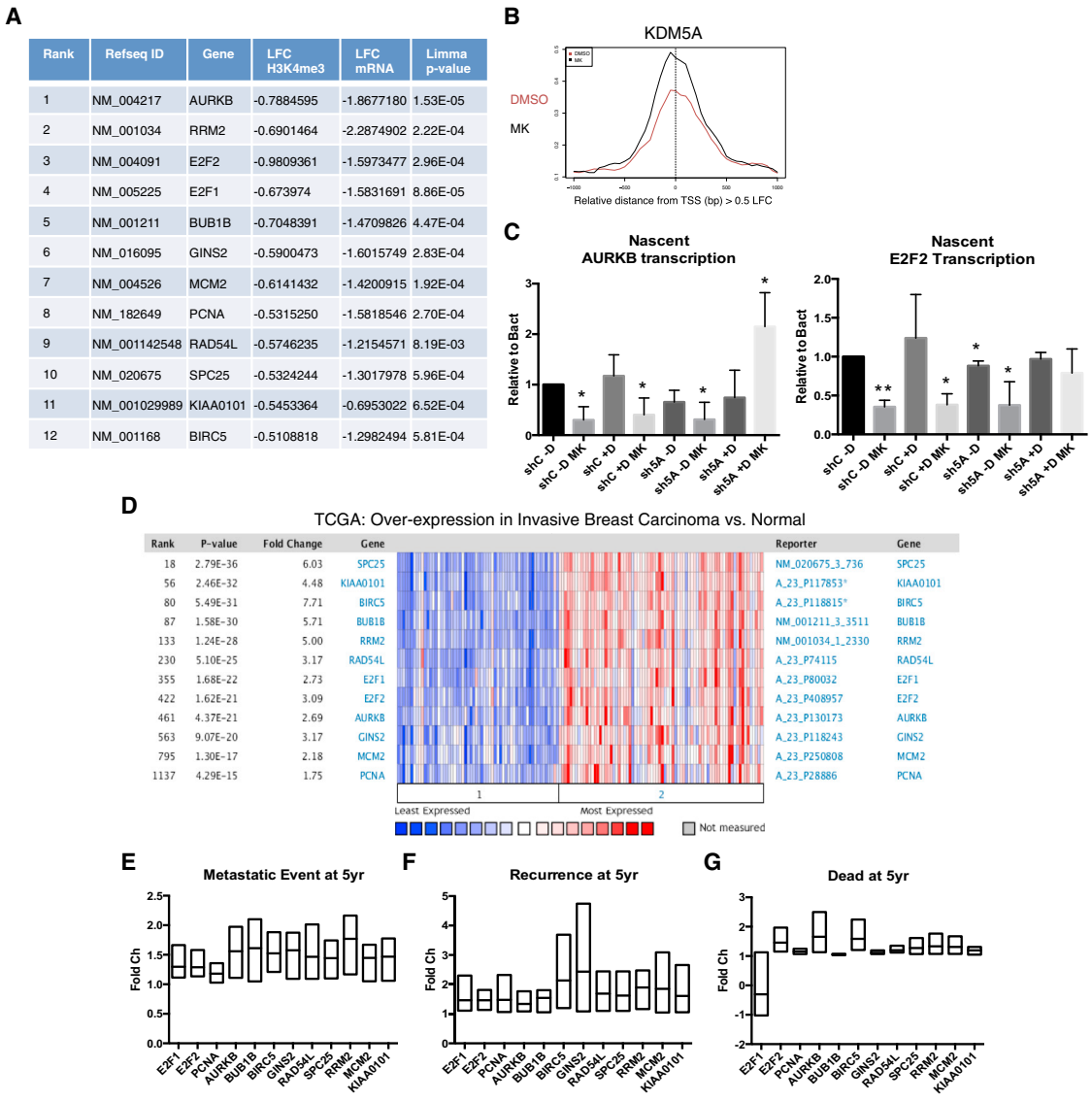

Figure 5. AKT/KDM5A-Regulated Gene Expression Is Elevated in Breast Cancer and Is a Predictor of Poor Clinical Outcome

(A) Table integrating H3K4me3 ChIP-seq, KDM5A ChIP-seq, and RNA-seq data from T47D cells treated with MK2206 (1 μM) for 24 hr.

(B) KDM5A wave plot of T47D cells treated with MK2206 (1 μM) representing all TSSs (69 total) also characterized by a ≥0.5 LFC in H3K4me3.

(C) T47D cells treated with doxycycline (2 mg/ml) for 48 hr and then MK2206 (1 μM) for 12 hr where indicated. Nascent RNA was isolated prior to qPCR within the *AURKB* and *E2F2* gene bodies. Data are shown as mean ± SEM. *$p \leq 0.05$ and **$p \leq 0.01$, Student's t test.

(D) Heat map representing Oncomine analysis of AKT/KDM5A regulated genes from Cancer Genome Atlas Network (2012) dataset.

(E) Correlation of mRNA expression of AKT/KDM5A-regulated genes and rate of patient metastatic event 5 years post-initial diagnosis. Analysis of three independent studies from Oncomine.

(F) Correlation of mRNA expression of AKT/KDM5A regulated genes and rate of patient breast cancer recurrence 5 years after initial diagnosis. Analysis of three independent studies from Oncomine.

(G) Correlation of mRNA expression of AKT/KDM5A regulated genes and rate of patient death 5 years after initial diagnosis. Analysis of three independent studies from Oncomine.

KDM5A knockdown fails to block AKT inhibition of H3K4me3 at the promoters of many AKT-regulated genes (data not shown). It is therefore possible that AKT regulates the function or activity of the homologous KDM5 enzymes KDM5B or KDM5C. Some genes identified here as AKT/5A-regulated genes are also KDM5B targets in breast cancer (Yamamoto et al., 2014). While KDM5B does not share any of the AKT consensus motifs mapped in KDM5A, two of the five residues implicated in AKT-mediated KDM5A phosphorylation are shared with KDM5C. The possibility that AKT modulates the function of histone methyl transferases in addition to KDM5A remains, which may also explain how AKT inhibition reduces H3K4me3 at the promoters

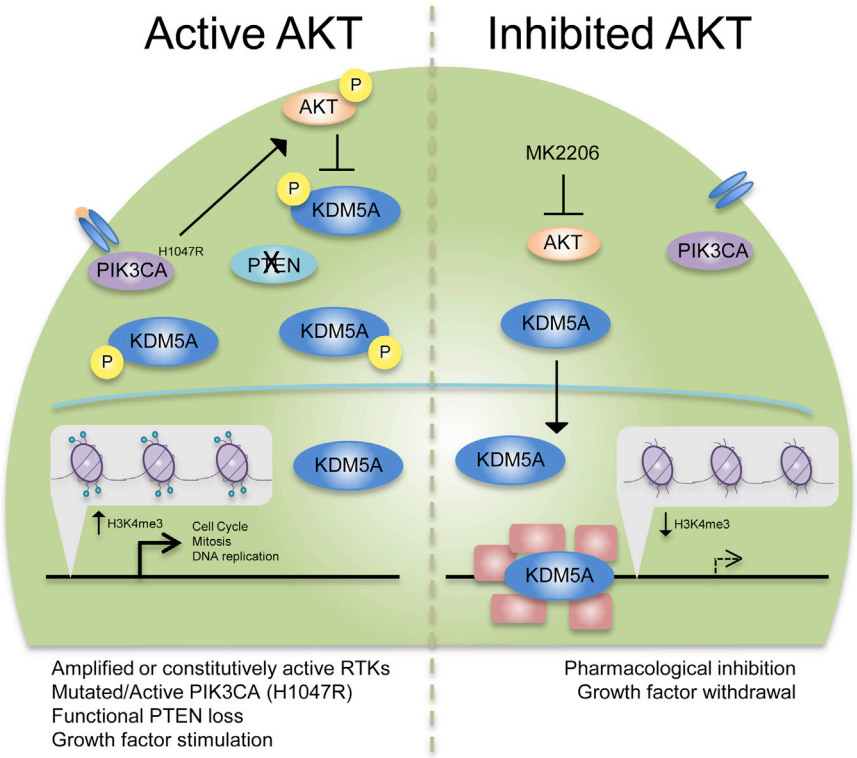

Figure 6. AKT Regulates Cell-Cycle-Promoting Genes through the Phosphorylation and Subcellular Redistribution of KDM5A

Left: Active PI3K/AKT signaling phosphorylates KDM5A and relocalizes KDM5A to the cytoplasm. Abundance of promoter-associated KDM5A is reduced, increasing TSS H3K4me3 and expression of AKT/5A-regulated genes.

Right: PI3K/AKT inhibition reduces AKT-mediated KDM5A phosphorylation, increasing KDM5A nuclear localization and promoter occupancy. Here, KDM5A demethylates H3K4me2/3 and reduces expression of cell-cycle-promoting genes.

of some AKT-regulated genes in the absence of KDM5A. Clearly, more research is needed to evaluate the ability of PI3K/AKT to cooperate with additional H3K4-directed demethylases and methyltransferases to regulate H3K4me3 and transcriptional competence.

Our findings suggest that H3K4 methylation is regulated by PI3K/AKT. H3K4me3 affects transcriptional competence and the expression of cell-cycle-promoting genes and is regulated at least in part by AKT/KDM5A. This information could be exploited in the development and preclinical testing of combination therapies using compounds directed at PI3K/AKT with novel compounds targeted to chromatin modifiers, such as MLL1/MEN1, in the treatment of PI3K-activated tumors. Our results suggest that reducing H3K4me3 through the chemical inhibition of the histone methyltransferase MLL1 may have therapeutic benefit in the treatment of PI3K-activated cancers. Indeed, preclinical studies demonstrate that MLL1/MEN1 inhibition reduces tumor growth in models of breast cancer with gain-of-function p53 mutations and in MLL-rearranged leukemias (Borkin et al., 2015; Zhu et al., 2015). Clearly, further studies are necessary to determine the therapeutic benefit in targeting these two important nodes within the PI3K pathway.

EXPERIMENTAL PROCEDURES

Cell Lines and Drugs

Cells were maintained at 37°C and 5% CO_2 in RPMI or DMEM + 10% FBS and Pen-Strep. MK2206, GDC-0941, BKM120, BYL719, KIN193, RAD001, CHIR, and MEK162 were purchased from Selleck.

Animal Models and In Vivo Treatment Studies

Formalin-fixed tumors originating from the previously characterized mammary specific, doxycycline-inducible human $PIK3CA^{H1047R}$ expressing mice (MMTV-rtTA, TetO-$PIK3CA^{H1047R}$; i$PIK3CA^{H1047R}$) were utilized for all experiments described (Liu et al., 2011). Doxycycline (dox; 2 mg/ml) was administered in drinking water. Where relevant, a fraction of the tumor was isolated followed with dox removal for 2 weeks prior to the isolation and preparation of the remaining tumor. Where applicable, GDC-0941 was reconstituted in 0.5% (wt/vol) methylcellulose and 0.2% Tween 80 and administered by oral gavage (125 mg/kg, once daily) for 7 days prior to tumor isolation and preparation. Tumors were isolated and prepared within 3 hr of the final treatment. All mouse experiments were conducted in accordance with protocols approved by the Institutional Animal Care and Use Committees (IACUCs) of Dana Farber Cancer Institute (DFCI) and Harvard Medical School (HMS).

Immunohistochemistry

Formalin-fixed, paraffin-embedded (FFPE) prepared tumors were sectioned (HMS Rodent Histopathology Core) and mounted. Sections were deparaffinized, hydrated, and antigens retrieved with sodium citrate. Following blocking of endogenous peroxidases, sections were blocked and incubated in primary antibody overnight (4°C). Primary antibodies used were as follows: AKTS473 (CST), H3K4me3 (Abcam), and KDM5A (Bethyl). Sections were washed and incubated in secondary antibody, after which they were incubated with ABC (Vector Labs), DAB developed (Vector Labs), and counter-stained with hematoxylin (Vector Labs). Sections were then dehydrated and mounted for imaging (Nikon Eclipse E600). KDM5A subcellular localization was quantified with blinded counting of cytoplasmic and nuclear KDM5A staining from more than 190 cells across three randomized images obtained from three separate mice per treatment group.

Cell Lysis and Immunoblotting

Cells were lysed in IP buffer (20 mM TrisHCl [pH 7.5], 150 mM NaCl, 5 mM $MgCl_2$, 1% NP-40) or fractionated (Pierce), supplemented with protease and phosphatase inhibitors. Histones were acid extracted by lysing in Triton extraction buffer (TEB; PBS, 0.5% Triton X-100) supplemented with protease inhibitors. Lysates were centrifuged 6,500 × *g* and histones were acid extracted from the resulting pellet with 1:1 TEB:0.8 M HCl. Histones were centrifuged and the supernatant precipitated with the addition of an equal volume of 50% TCA, then 12,000 × *g* centrifugation. Histones were washed one time in 0.3 M HCl in acetone and two times in 100% acetone before vacuum drying and resuspended in 20 μM Tris-HCl (pH 8.0). Whole cell lysate, fractionated lysate, or acid-extracted proteins were separated using SDS-PAGE. Proteins were transferred to nitrocellulose membranes and blocked in TBST+5% milk.

Proteins of interest were visualized and quantified after primary antibody incubation (Odyssey, Li-Cor). Primary antibodies used were as follows: AKT, AKTS473, AKTT308, S6, S6S240/44, BUB1B, AURKB, HA (CST), β-actin (Millipore), KDM5A (Bethyl), H3, H3K4me3, H3K4me2, H3K4me, pS/T (Abcam), E2F1, E2F2, PCNA (Santa Cruz), FlagM2, and α-tubulin (Sigma).

ChIP and ChIP-Seq

H3K4me3 ChIP was performed in T47D cells with 2.5 × 10^6 cells/IP, as previously described (Carroll et al., 2005). In brief, cells were treated as indicated. Cells were crosslinked, lysed in SDS lysis buffer, and sonicated (Covaris). H3K4me3 antibody (3 μg) was added to sonicated lysates per overnight (o/n) IP. Protein A beads (Novex) were incubated with IP for 6 hr. Chromatin was eluted and reverse crosslinked o/n and DNA was recovered with RNase A incubation. Glycogen and proteinase K were added and incubated at 62°C. DNA was purified and eluted in Low TE. KDM5A and HA ChIPs were performed using the Sarkosyl method (Lee et al., 2006) with 2.5 × 10^8 cells/ChIP and KDM5A #1416 antibody (10 μg) (Dr. William Kaelin) or HA ab9110 (5 μg) (Abcam), respectively.

For samples that were Illumina sequenced, ChIP eluate was purified (Ampure) and indices added (ThruPLEX-FD Prep kit, Rubicon Genomics). Samples were then size selected (Pippin Prep, Sage Science) and purified (Ampure). DNA quality and quantity was measured using a Fragment Bioanalyzer and samples submitted to the Center for Functional Cancer Epigenetics for sequencing on a Next-Seq Illumina platform.

RNA Isolation and qPCR

T47D cells were treated as described and RNA isolated (QIAGEN). Nascent RNA isolation was performed according to manufacturer's instructions (Life Technologies). cDNA was synthesized using iScript (BioRad) and amplified (ABI7300).

Bioinformatics

Human genome build 19 (hg19) was used as the reference genome. RNA-seq data were aligned using Tophat and further analyzed using Cufflinks and Limma for expression analysis (Ritchie et al., 2015; Trapnell et al., 2009, 2010). Gene set enrichment analysis was performed using the online tool from the Broad Institute (Mootha et al., 2003). Boxplots were made in Bioconductor/R. To determine significant differences in transcript expression, a two-tailed unpaired or paired (whichever appropriate) Student's t test was used, and a two-sided p value of <0.05 was considered significant. Sequencing data from ChIP experiments was aligned to hg19 using Bowtie (Langmead et al., 2009). For peak calling, MACS2 was used (Feng et al., 2012). For intersecting peak data, we used the Table Browser at the UCSC genome bioinformatics web site (http://genome.ucsc.edu/). The mapBam.py script to map reads from a bam to a gff file was used to determine quantitative fold changes in H3K4me3 after MK treatment (Lovén et al., 2013). For the integrative analysis, TSS with KDM5A ChIP-seq peaks after MK treatment were filtered for those showing a significant reduction in H3K4me3 (>0.5 log2 fold down) following MK treatment. These genes were further refined for those also showing a significant decrease in mRNA levels (>0.5 log2 fold down, $p < 0.01$). For k-means clustering of ChIP-seq data and drawing average ChIP-seq scores (SitePro), we used the integrative tools that can be found at http://www.cistrome.org (Liu et al., 2011).

Immunofluorescence

Cos7 cells were seeded over glass coverslips and transfected with the indicated plasmid. Cells were treated as described and fixed in 4% paraformaldehyde and permeabilized in 0.1% Triton X-100 in 1 mM glycine. Coverslips were incubated with FlagM2 (Sigma), washed, and incubated with alexa-488 (Invitrogen). Nuclei were stained with 0.5 μg/ml Hoechst (Invitrogen), after which coverslips were mounted for imaging using an 80i Nikon epifluorescent microscope (Nikon Imaging Center, Harvard Medical School).

IP/Kinase Assay

293T cells were transfected with pBabeHA-FLAG-KDM5A (Dr. William Kaelin) or pBabeHA-FLAG-KDM5A^{mut5A} and then lysed in IP buffer for subsequent IP with Flag-agarose beads (Sigma). Beads were washed and resuspended in kinase assay buffer (0.2M TrisHCl [pH 7.5], 0.005M $MgCl_2$), protease and phosphatase inhibitors, and DMSO or 2 μM MK2206. Each reaction received 2.5 μCi γ^{32}P-ATP and recombinant purified AKT1 (ProQinase). Reactions were incubated 30°C for 30 min, and proteins were separated by SDS-PAGE. SDS-PAGE gels were then fixed and kinase assays imaged using phosphorescence (Typhoon Trio, GE).

Statistical Analysis

Western blot, biochemical fractionation, ChIP-qPCR, qPCR, and IHC assays were performed in three independent experiments unless otherwise noted. Mean ± SEM are reported. Statistical significance ($p < 0.05$) of differences between two groups was determined by Student's t test.

ACCESSION NUMBERS

The accession number for the data generated in this paper is GEO: GSE80594.

SUPPLEMENTAL INFORMATION

Supplemental Information includes Supplemental Experimental Procedures and five figures and can be found with this article online at http://dx.doi.org/10.1016/j.celrep.2016.05.046.

AUTHOR CONTRIBUTIONS

J.M.S., T.M.R., and M.B. designed the research. J.M.S., K.M.D., A.C.G., H.C., and C.O. performed the research. C.Y.L., J.R., and J.B. contributed novel analytic tools. J.M.S., K.M.D., A.C.G., C.Y.L., and J.R. analyzed the data. M.B., T.M.R., J.J.Z., and J.B. supervised the studies. J.M.S., K.M.D., T.M.R., and M.B. wrote the manuscript.

ACKNOWLEDGMENTS

We thank Dr. W. Kaelin (DFCI) for generously providing the pBabeHA-FLAG-KDM5A plasmid and the KDM5A #1416 antibody, Drs. Y. Shi and A. Heilmann for project discussions, and I. Koutsopatriy for technical assistance. This study was supported in part by grants from the NIH (5-P50-CA168504-03 to T.M.R. and J.J.Z.), the American Cancer Society (125303-PF-13-097-01-CCE to J.M.S.), the Dutch Cancer Society (UU2012-5370 to K.M.D.), and Susan G. Komen (to M.B.).

Received: October 26, 2015
Revised: February 25, 2016
Accepted: May 10, 2016
Published: June 9, 2016

REFERENCES

Benard, A., Goossens-Beumer, I.J., van Hoesel, A.Q., de Graaf, W., Horati, H., Putter, H., Zeestraten, E.C., van de Velde, C.J., and Kuppen, P.J. (2014). Histone trimethylation at H3K4, H3K9 and H4K20 correlates with patient survival and tumor recurrence in early-stage colon cancer. BMC Cancer *14*, 531.

Benevolenskaya, E.V., Murray, H.L., Branton, P., Young, R.A., and Kaelin, W.G., Jr. (2005). Binding of pRB to the PHD protein RBP2 promotes cellular differentiation. Mol. Cell *18*, 623–635.

Borkin, D., He, S., Miao, H., Kempinska, K., Pollock, J., Chase, J., Purohit, T., Malik, B., Zhao, T., Wang, J., et al. (2015). Pharmacologic inhibition of the Menin-MLL interaction blocks progression of MLL leukemia in vivo. Cancer Cell *27*, 589–602.

Brunet, A., Bonni, A., Zigmond, M.J., Lin, M.Z., Juo, P., Hu, L.S., Anderson, M.J., Arden, K.C., Blenis, J., and Greenberg, M.E. (1999). Akt promotes cell survival by phosphorylating and inhibiting a Forkhead transcription factor. Cell *96*, 857–868.

Cancer Genome Atlas Network (2012). Comprehensive molecular portraits of human breast tumours. Nature *490*, 61–70.

Cao, F., Townsend, E.C., Karatas, H., Xu, J., Li, L., Lee, S., Liu, L., Chen, Y., Ouillette, P., Zhu, J., et al. (2014a). Targeting MLL1 H3K4 methyltransferase activity in mixed-lineage leukemia. Mol. Cell *53*, 247–261.

Cao, J., Liu, Z., Cheung, W.K., Zhao, M., Chen, S.Y., Chan, S.W., Booth, C.J., Nguyen, D.X., and Yan, Q. (2014b). Histone demethylase RBP2 is critical for breast cancer progression and metastasis. Cell Rep. *6*, 868–877.

Carroll, J.S., Liu, X.S., Brodsky, A.S., Li, W., Meyer, C.A., Szary, A.J., Eeckhoute, J., Shao, W., Hestermann, E.V., Geistlinger, T.R., et al. (2005). Chromosome-wide mapping of estrogen receptor binding reveals long-range regulation requiring the forkhead protein FoxA1. Cell *122*, 33–43.

Cha, T.L., Zhou, B.P., Xia, W., Wu, Y., Yang, C.C., Chen, C.T., Ping, B., Otte, A.P., and Hung, M.C. (2005). Akt-mediated phosphorylation of EZH2 suppresses methylation of lysine 27 in histone H3. Science *310*, 306–310.

Christensen, J., Agger, K., Cloos, P.A., Pasini, D., Rose, S., Sennels, L., Rappsilber, J., Hansen, K.H., Salcini, A.E., and Helin, K. (2007). RBP2 belongs to a family of demethylases, specific for tri-and dimethylated lysine 4 on histone 3. Cell *128*, 1063–1076.

Engelman, J.A., Luo, J., and Cantley, L.C. (2006). The evolution of phosphatidylinositol 3-kinases as regulators of growth and metabolism. Nat. Rev. Genet. *7*, 606–619.

Feng, J., Liu, T., Qin, B., Zhang, Y., and Liu, X.S. (2012). Identifying ChIP-seq enrichment using MACS. Nat. Protoc. *7*, 1728–1740.

Ge, Z., Li, W., Wang, N., Liu, C., Zhu, Q., Björkholm, M., Gruber, A., and Xu, D. (2010). Chromatin remodeling: recruitment of histone demethylase RBP2 by Mad1 for transcriptional repression of a Myc target gene, telomerase reverse transcriptase. FASEB J. *24*, 579–586.

Gera, J.F., Mellinghoff, I.K., Shi, Y., Rettig, M.B., Tran, C., Hsu, J.H., Sawyers, C.L., and Lichtenstein, A.K. (2004). AKT activity determines sensitivity to mammalian target of rapamycin (mTOR) inhibitors by regulating cyclin D1 and c-myc expression. J. Biol. Chem. *279*, 2737–2746.

Hamamoto, R., Saloura, V., and Nakamura, Y. (2015). Critical roles of non-histone protein lysine methylation in human tumorigenesis. Nat. Rev. Cancer *15*, 110–124.

Hou, J., Wu, J., Dombkowski, A., Zhang, K., Holowatyj, A., Boerner, J.L., and Yang, Z.Q. (2012). Genomic amplification and a role in drug-resistance for the KDM5A histone demethylase in breast cancer. Am. J. Transl. Res. *4*, 247–256.

Jiping, Z., Ming, F., Lixiang, W., Xiuming, L., Yuqun, S., Han, Y., Zhifang, L., Yundong, S., Shili, L., Chunyan, C., and Jihui, J. (2013). MicroRNA-212 inhibits proliferation of gastric cancer by directly repressing retinoblastoma binding protein 2. J. Cell. Biochem. *114*, 2666–2672.

Junttila, T.T., Akita, R.W., Parsons, K., Fields, C., Lewis Phillips, G.D., Friedman, L.S., Sampath, D., and Sliwkowski, M.X. (2009). Ligand-independent HER2/HER3/PI3K complex is disrupted by trastuzumab and is effectively inhibited by the PI3K inhibitor GDC-0941. Cancer Cell *15*, 429–440.

Juric, D., Castel, P., Griffith, M., Griffith, O.L., Won, H.H., Ellis, H., Ebbesen, S.H., Ainscough, B.J., Ramu, A., Iyer, G., et al. (2015). Convergent loss of PTEN leads to clinical resistance to a PI(3)Kα inhibitor. Nature *518*, 240–244.

Kandoth, C., McLellan, M.D., Vandin, F., Ye, K., Niu, B., Lu, C., Xie, M., Zhang, Q., McMichael, J.F., Wyczalkowski, M.A., et al. (2013). Mutational landscape and significance across 12 major cancer types. Nature *502*, 333–339.

Klose, R.J., Yan, Q., Tothova, Z., Yamane, K., Erdjument-Bromage, H., Tempst, P., Gilliland, D.G., Zhang, Y., and Kaelin, W.G., Jr. (2007). The retinoblastoma binding protein RBP2 is an H3K4 demethylase. Cell *128*, 889–900.

Kopan, R., and Ilagan, M.X. (2009). The canonical Notch signaling pathway: unfolding the activation mechanism. Cell *137*, 216–233.

Langmead, B., Trapnell, C., Pop, M., and Salzberg, S.L. (2009). Ultrafast and memory-efficient alignment of short DNA sequences to the human genome. Genome Biol. *10*, R25.

Lee, T.I., Johnstone, S.E., and Young, R.A. (2006). Chromatin immunoprecipitation and microarray-based analysis of protein location. Nat. Protoc. *1*, 729–748.

Liefke, R., Oswald, F., Alvarado, C., Ferres-Marco, D., Mittler, G., Rodriguez, P., Dominguez, M., and Borggrefe, T. (2010). Histone demethylase KDM5A is an integral part of the core Notch-RBP-J repressor complex. Genes Dev. *24*, 590–601.

Liu, P., Cheng, H., Santiago, S., Raeder, M., Zhang, F., Isabella, A., Yang, J., Semaan, D.J., Chen, C., Fox, E.A., et al. (2011). Oncogenic PIK3CA-driven mammary tumors frequently recur via PI3K pathway-dependent and PI3K pathway-independent mechanisms. Nat. Med. *17*, 1116–1120.

Liu, Y., Liu, F., Yu, H., Zhao, X., Sashida, G., Deblasio, A., Harr, M., She, Q.B., Chen, Z., Lin, H.K., et al. (2012). Akt phosphorylates the transcriptional repressor bmi1 to block its effects on the tumor-suppressing ink4a-arf locus. Sci. Signal. *5*, ra77.

Liu, P., Begley, M., Michowski, W., Inuzuka, H., Ginzberg, M., Gao, D., Tsou, P., Gan, W., Papa, A., Kim, B.M., et al. (2014). Cell-cycle-regulated activation of Akt kinase by phosphorylation at its carboxyl terminus. Nature *508*, 541–545.

Lopez-Bigas, N., Kisiel, T.A., Dewaal, D.C., Holmes, K.B., Volkert, T.L., Gupta, S., Love, J., Murray, H.L., Young, R.A., and Benevolenskaya, E.V. (2008). Genome-wide analysis of the H3K4 histone demethylase RBP2 reveals a transcriptional program controlling differentiation. Mol. Cell *31*, 520–530.

Lovén, J., Hoke, H.A., Lin, C.Y., Lau, A., Orlando, D.A., Vakoc, C.R., Bradner, J.E., Lee, T.I., and Young, R.A. (2013). Selective inhibition of tumor oncogenes by disruption of super-enhancers. Cell *153*, 320–334.

Luo, J., Su, F., Chen, D., Shiloh, A., and Gu, W. (2000). Deacetylation of p53 modulates its effect on cell growth and apoptosis. Nature *408*, 377–381.

Manning, B.D., and Cantley, L.C. (2007). AKT/PKB signaling: navigating downstream. Cell *129*, 1261–1274.

Meier, R., Alessi, D.R., Cron, P., Andjelković, M., and Hemmings, B.A. (1997). Mitogenic activation, phosphorylation, and nuclear translocation of protein kinase Bbeta. J. Biol. Chem. *272*, 30491–30497.

Mootha, V.K., Lindgren, C.M., Eriksson, K.F., Subramanian, A., Sihag, S., Lehar, J., Puigserver, P., Carlsson, E., Ridderstråle, M., Laurila, E., et al. (2003). PGC-1alpha-responsive genes involved in oxidative phosphorylation are coordinately downregulated in human diabetes. Nat. Genet. *34*, 267–273.

Mungamuri, S.K., Murk, W., Grumolato, L., Bernstein, E., and Aaronson, S.A. (2013). Chromatin modifications sequentially enhance ErbB2 expression in ErbB2-positive breast cancers. Cell Rep. *5*, 302–313.

Obenauer, J.C., Cantley, L.C., and Yaffe, M.B. (2003). Scansite 2.0: proteome-wide prediction of cell signaling interactions using short sequence motifs. Nucleic Acids Res. *31*, 3635–3641.

Rhodes, D.R., Yu, J., Shanker, K., Deshpande, N., Varambally, R., Ghosh, D., Barrette, T., Pandey, A., and Chinnaiyan, A.M. (2004). ONCOMINE: a cancer microarray database and integrated data-mining platform. Neoplasia *6*, 1–6.

Ritchie, M.E., Phipson, B., Wu, D., Hu, Y., Law, C.W., Shi, W., and Smyth, G.K. (2015). limma powers differential expression analyses for RNA-sequencing and microarray studies. Nucleic Acids Res. *43*, e47.

Rodon, J., Dienstmann, R., Serra, V., and Tabernero, J. (2013). Development of PI3K inhibitors: lessons learned from early clinical trials. Nat. Rev. Clin. Oncol. *10*, 143–153.

Rokudai, S., Laptenko, O., Arnal, S.M., Taya, Y., Kitabayashi, I., and Prives, C. (2013). MOZ increases p53 acetylation and premature senescence through its complex formation with PML. Proc. Natl. Acad. Sci. USA *110*, 3895–3900.

Santos-Rosa, H., Schneider, R., Bannister, A.J., Sherriff, J., Bernstein, B.E., Emre, N.C., Schreiber, S.L., Mellor, J., and Kouzarides, T. (2002). Active genes are tri-methylated at K4 of histone H3. Nature *419*, 407–411.

Secombe, J., Li, L., Carlos, L., and Eisenman, R.N. (2007). The Trithorax group protein Lid is a trimethyl histone H3K4 demethylase required for dMyc-induced cell growth. Genes Dev. *21*, 537–551.

Sharma, S.V., Lee, D.Y., Li, B., Quinlan, M.P., Takahashi, F., Maheswaran, S., McDermott, U., Azizian, N., Zou, L., Fischbach, M.A., et al. (2010). A chromatin-mediated reversible drug-tolerant state in cancer cell subpopulations. Cell *141*, 69–80.

Songyang, Z., Blechner, S., Hoagland, N., Hoekstra, M.F., Piwnica-Worms, H., and Cantley, L.C. (1994). Use of an oriented peptide library to determine the optimal substrates of protein kinases. Curr. Biol. *4*, 973–982.

Thorpe, L.M., Yuzugullu, H., and Zhao, J.J. (2015). PI3K in cancer: divergent roles of isoforms, modes of activation and therapeutic targeting. Nat. Rev. Cancer *15*, 7–24.

Trapnell, C., Pachter, L., and Salzberg, S.L. (2009). TopHat: discovering splice junctions with RNA-Seq. Bioinformatics *25*, 1105–1111.

Trapnell, C., Williams, B.A., Pertea, G., Mortazavi, A., Kwan, G., van Baren, M.J., Salzberg, S.L., Wold, B.J., and Pachter, L. (2010). Transcript assembly and quantification by RNA-Seq reveals unannotated transcripts and isoform switching during cell differentiation. Nat. Biotechnol. *28*, 511–515.

Wei, Y., Xia, W., Zhang, Z., Liu, J., Wang, H., Adsay, N.V., Albarracin, C., Yu, D., Abbruzzese, J.L., Mills, G.B., et al. (2008). Loss of trimethylation at lysine 27 of histone H3 is a predictor of poor outcome in breast, ovarian, and pancreatic cancers. Mol. Carcinog. *47*, 701–706.

Xu, K., Wu, Z.J., Groner, A.C., He, H.H., Cai, C., Lis, R.T., Wu, X., Stack, E.C., Loda, M., Liu, T., et al. (2012). EZH2 oncogenic activity in castration-resistant prostate cancer cells is Polycomb-independent. Science *338*, 1465–1469.

Yamamoto, S., Wu, Z., Russnes, H.G., Takagi, S., Peluffo, G., Vaske, C., Zhao, X., Moen Vollan, H.K., Maruyama, R., Ekram, M.B., et al. (2014). JARID1B is a luminal lineage-driving oncogene in breast cancer. Cancer Cell *25*, 762–777.

Zeng, J., Ge, Z., Wang, L., Li, Q., Wang, N., Björkholm, M., Jia, J., and Xu, D. (2010). The histone demethylase RBP2 Is overexpressed in gastric cancer and its inhibition triggers senescence of cancer cells. Gastroenterology *138*, 981–992.

Zhu, J., Sammons, M.A., Donahue, G., Dou, Z., Vedadi, M., Getlik, M., Barsyte-Lovejoy, D., Al-awar, R., Katona, B.W., Shilatifard, A., et al. (2015). Gain-of-function p53 mutants co-opt chromatin pathways to drive cancer growth. Nature *525*, 206–211.